processes

Article

Experimental Study on the Performance-Influencing Factors of an Aviation Heavy-Oil Two-Stroke Direct-Injection Ignition Engine

Bo Lu [1], Taixue Bei [1,*], Rui Liu [2], Na Liu [1], Ying Luo [1] and Yuchen Liu [1]

[1] School of Mechanical and Electrical Engineering, Shandong Jianzhu University, Jinan 250101, China
[2] School of Mechanical and Power Engineering, Nanjing Tech University, Nanjing 211816, China
* Correspondence: 13709@sdjzu.edu.cn

Abstract: To study the influence of control parameters under cold-start and low-load conditions on the performance of a heavy-oil, two-stroke, direct-injection, ignition engine for use in aviation, the operation of a two-stroke, direct-injection engine was studied in a bench test. The results were as follows: ① When the ambient temperature is 15 °C, the battery voltage is 12.4 V, and the peak speed of the starting motor is 1200 r/min. As the concentration factor increases, the cold-start speed increases, and the fuel consumption increases. The influence on the cold start is reduced after reaching a certain concentration. The cold-start time decreases with the increasing magnetization pulse width. The cold-start time is the shortest at an oil–gas interval of 6 ms. ② Under small-load conditions of 3000 r/min and 14% to 16% throttle, a higher ignition energy increases the engine power. Pollutant emissions are the lowest when the fuel injection is 7.5 mg and the excess air coefficient is approximately 1.1.

Keywords: two-stroke direct-injection kerosene engine; cold start; small load conditions; oil–gas interval; excess air coefficient

Citation: Lu, B.; Bei, T.; Liu, R.; Liu, N.; Luo, Y.; Liu, Y. Experimental Study on the Performance-Influencing Factors of an Aviation Heavy-Oil Two-Stroke Direct-Injection Ignition Engine. *Processes* **2022**, *10*, 2646. https://doi.org/10.3390/pr10122646

Academic Editors: Dezhi Zhou and Jing Li

Received: 4 November 2022
Accepted: 6 December 2022
Published: 8 December 2022

1. Introduction

Since Bartra made the world's first two-stroke engine more than 100 years ago, two-stroke engines have become the most widely used thermal power machinery, with a high thermal efficiency and power-to-weight ratio, as a result of the continuous improvements in combustion technology and electronic control technology [1,2]. Compared with a four-stroke engine, a two-stroke engine with the same displacement has a higher mechanical efficiency, smaller rotational inertia, and larger amount of power per liter, which are consistent with the high endurance requirements of UAVs. A two-stroke, air-cooled engine can also achieve a reverse arrangement, so it is widely used in medium and small UAVs [3,4].

Heavy oil is a product of petroleum fractionation. The utility model of an engine is characterized by fuel with a suitable density, a high heat value, good combustibility, and good low-temperature fluidity, and such engines have been researched and applied in jet engines. However, there have been few studies on two-stroke, kerosene engines. Some vehicles that are normally fueled by gasoline have also been fueled by alternative fuels, mainly kerosene and diesel oil [5]. For example, specialized vehicles in military applications have used a single fuel that is easy to store and transport in all vehicles and equipment, rather than different fuels for different equipment, thus increasing safety [6]. The diesel engine is representative of traditional heavy-oil engines but has obvious disadvantages, such as a high fuel consumption and poor cold-start performance. An ignited heavy-oil engine possesses the advantages of a gasoline engine, such as a high power-weight ratio, a small size, and little vibration. Burning heavy oil in early ignition, reciprocating engines has been attempted. However, the spark plugs developed serious carbon deposits, and the engine exhibited a poor cold-start performance and could not perform satisfactorily in the full-load rpm range. These disadvantages limit the use of heavy-oil, two-stroke engines, so it is important to study the factors affecting their performance.

2. Domestic and International Status Quo

The development of heavy-oil ignition engines began in the late 1980s, initially only as compression, ignition engines used in military vehicles that burn aviation kerosene and then gradually extending to outboard motorboats and aviation UAV power plant applications [7,8].

2.1. Traditional Heavy-Oil, Ignition, Piston Engine

Since the 1990s, the traditional heavy-oil, ignition, piston engine has been widely used by the military in Europe and the United States. After 2000, some foreign, private engine companies or related state-owned research institutions gradually launched heavy-oil, ignition engine products, usually called heavy-fuel engines (HFEs) or multifuel engines (MFEs) [9,10]. Table 1 shows some product models of heavy-oil, ignition, piston engines with inlet injections.

Table 1. Heavy-oil, ignition, piston engine with an inlet injection mode.

Engine Manufacturer	**3W**	**Northwest**	**Sonex**	**RCV**	**Rotron**
Engine type	Two-stroke	Two-stroke	Two-stroke	Four-stroke	Rotor piston
Representative	3W-56i B2 HFE FI	NW-44 EFI MFE	SONEX 3W240 HFE	RCV DF70 MFE	Rotron RT300 HFE
Engine picture					
Displacement (cm^3)	56	44	240	70	300
Weight (kg)	2.6	1.02	6.7	2.7	12.3
Power rate (kW)	4.0	3.0	16.5	4.1	23.1
Cooling type	Air-cooled	Air-cooled	Air-cooled	Air-cooled	Water-cooled
Usable fuel	JP5/JP8/JET A1	JP5/JP8/JET A1	JP5/JP8/Gasoline	JP5/JP8/JET A1	JP5/JP8/JET A1

2.2. Heavy-Oil, Direct-Injection, Ignition, Piston Engine

Engine enterprises, research institutes, and institutions of higher learning outside of China focused on heavy-oil, direct-injection, ignition engines in the early 21st century and then began systematic research on such engines before gradually launching a series of heavy-oil, direct-injection, ignition engines [11]. China is still in its infancy in this field and has not yet launched any similar products. Table 2 shows a heavy-oil, two-stroke, direct-injection, spark-ignition, piston engine from the Hirth Company in Germany.

Table 2. Heavy-oil, two-stroke, direct-injection, spark-ignition, piston engine produced by the Hirth Company, Germany.

Engine photographs				
Representative	S4102	S1200	S1204	3503HF
Engine type	Dual-cylinder	Dual-cylinder opposed	Dual-cylinder opposed	Dual-cylinder in line
Displacement (cm^3)	65	130	500	625
Weight (kg)	3.0	4.5	22	38
Power rate (kW)	5	10	33	45
Cooling type	Air-cooled	Air-cooled	Air-cooled	Water-cooled
Usable fuel	JP8/Jet A1	JP5/JP8/Jet A1	JP5/JP8/Jet A1	JP5/JP8/Jet A1

2.3. Research on the Parameters Controlling the Fuel Injection and Ignition System of an Ignition, Piston Engine

Research on the fuel injection system and ignition system are important for the continued development of spark-ignition, piston engines. Table 3 shows a comparison of heavy-oil, two-stroke, direct-injection, ignition engines for multiple applications.

Table 3. Comparison of heavy-oil, two-stroke, direct-injection, ignition engines in multiple applications.

Engine photograph					
Company	Mercury	Barrus	Evinrude	Zanzottera	Ricardo
Engine type	Two-stroke	Two-stroke	Two-stroke	Two-stroke	Two-stroke
Displacement (cm^3)	3032	697	577	498	88
Power rate (kW)	136	34.4	22.4	32.8	2.3
Cooling type	Water-cooled	Water-cooled	Water-cooled	Air-cooled	Air-cooled
Ignition method	Digital inductance	Digital capacitance	Digital inductance	Digital inductance	Digital inductance
Usable fuel	JP5/JP8/ Jet A1	Gasoline/JP5/ JP8/Diesel	Gasoline/JP5/ JP8	Gasoline/JP5/ JP8	Gasoline/JP5/ JP8

Hu Chunming et al. from Tianjin University studied the effects of parameters such as the oil and gas intervals on combustion stability during a cold start on a low-pressure, air-assisted, direct-injection, kerosene engine bench [12]. Wang Hu et al. studied the effects of different parameters on engine knock intensity and average effective pressure by numerical simulation [13]. Liu Rui studied the combustion characteristics of aviation kerosene (PR-3) at different loads on a four-stroke diesel engine [14] and the cold-start strategy of the two-stroke engine [15]. In summary, there are relatively extensive studies from China on the factors influencing the performance of gasoline and diesel engines. Research in other countries has mainly focused on engine performance under different fuel mixing conditions [16,17], but there are few studies on two-stroke, kerosene engines for use in aviation. Therefore, it is important to study the factors influencing the performance of heavy-oil, two-stroke, direct-injection, ignition engines for use in aviation. In this study, the variable parameters are studied by using a test bench to provide a reference for related fields.

3. Test System Construction

Table 4 shows a comparison of the main characteristics of gasoline, diesel, and RP-3 aviation kerosene. Table 5 shows the test equipment and instruments used for testing.

Table 4. Comparison of the main characteristics of gasoline, diesel, and RP-3 aviation kerosene.

Physicochemical Properties	Gasoline	Diesel	RP-3 Aviation Kerosene
Composition	C_5~C_{11}	C_{15}~C_{23}	C_7~C_{16}
Molecular weight	114	180~200	141
Liquid density (kg/L)	0.70~0.75	0.82~0.88	0.73~0.82
Solidification point (°C)	−80	−50	−60
Boiling point (°C)	25~220	160~360	147~230
Self-ignition temperature (°C)	220~250	350~380	275
Flash point (°C)	−45	50~65	35~51
Vapor pressure (kPa) (38 °C)	49~83	–	6
Concentration limit of the ignition flame (vol%)	1.4~7.6	1.58~8.2	0.71~5.19
Kinematic viscosity (mm^2/s) (20 °C)	0.62	2.5	1.25
Surface tension (10^{-3} N/m) (20 °C)	21.6	27	23.6
Theoretical air–fuel ratio	14.82	14.40	14.65
Latent heat of vaporization (kJ/kg)	310~350	375	353~361
Lower calorific value (kJ/kg)	44,000	43,250	43,350
Heat value of mixture (kJ/kmol)	84,467	83,962	84,423

Table 5. Test equipment and instruments.

Instrument Name	Model/Type	Manufacturer
Dynamometer	CW110G	Complant
Throttle position sensor	Linear output type	Bosch
Cylinder block temperature sensor	NTC thermistor (10 K)	Advantech
Atmospheric temperature sensor	NTC thermistor (10 K)	Advantech
Intake pressure sensor	Linear output type	Delphi
Engine speed sensor	Grooved photoelectric switch	Shinkon
Oil/gas pressure sensor	MIK-P300	Meacon
Cylinder pressure sensor	6113B	Kistler
Air–fuel ratio analyzer	LM-2	Ecotrons
Exhaust gas analyzer	FGA-4100	FGA
Fuel consumption meter	YHW-010	Complant

3.1. Test Electrical Control System

The electronic control system of an engine is mainly composed of sensors, ECUs, and actuators. A structure diagram is shown in Figure 1, and the timing of fuel injection and the application of ignition parameters is shown in Figure 2.

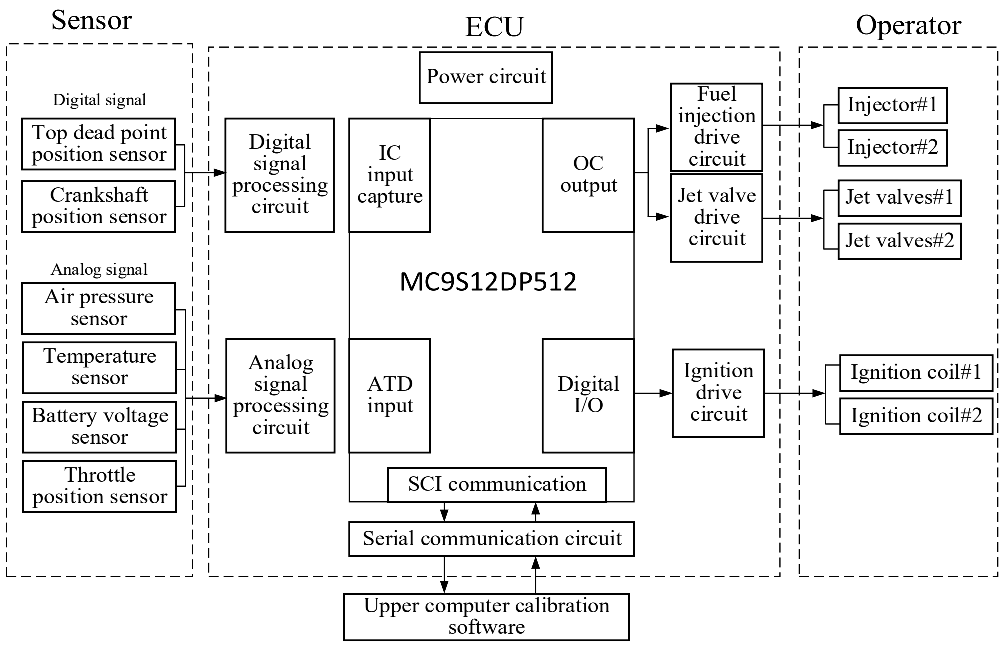

Figure 1. Structure block diagram of the prototype electronic control system.

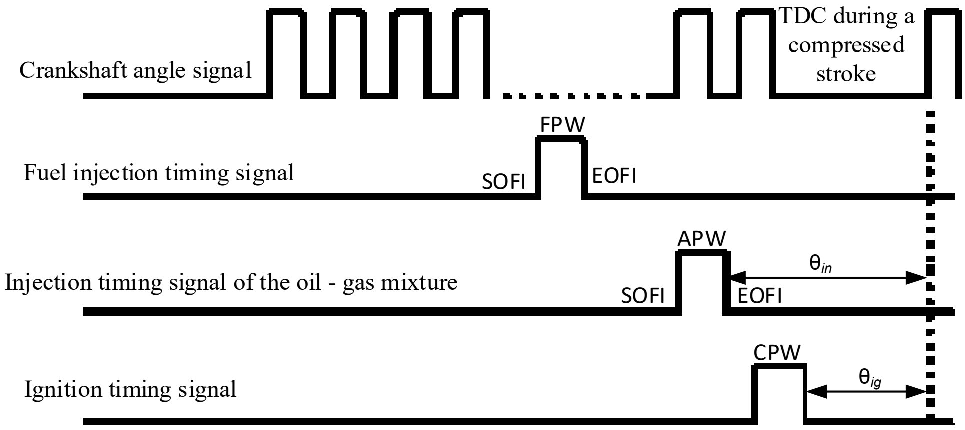

Figure 2. Timing diagram for the fuel injection and ignition parameters.

The abbreviations in Figure 2 correspond to the following parameters: fuel pulse width, FPW; start of fuel injection, SOFI; end of fuel injection, EOFI; air pulse width, APW; start of air injection, SOAI; end of air injection, EOAI; charge pulse width, CPW.

3.1.1. Microcontroller

The microcontroller is the core of the control system of a two-stroke, direct-injection engine. In this study, an MC9S12DP512 microcontroller with a 12-core CPU (Star Core) and 25 MHs bus speed is adopted. The advantages of this controller are a low clock frequency, high noise, and high vibration. The laboratory environment and the large memory can quickly realize complex mathematical operations to accurately control the parameters in the test.

3.1.2. Power Circuit

The function of the power circuit is to provide a stable power supply to the ECU, sensors, and actuators. Figure 3 shows the power circuit.

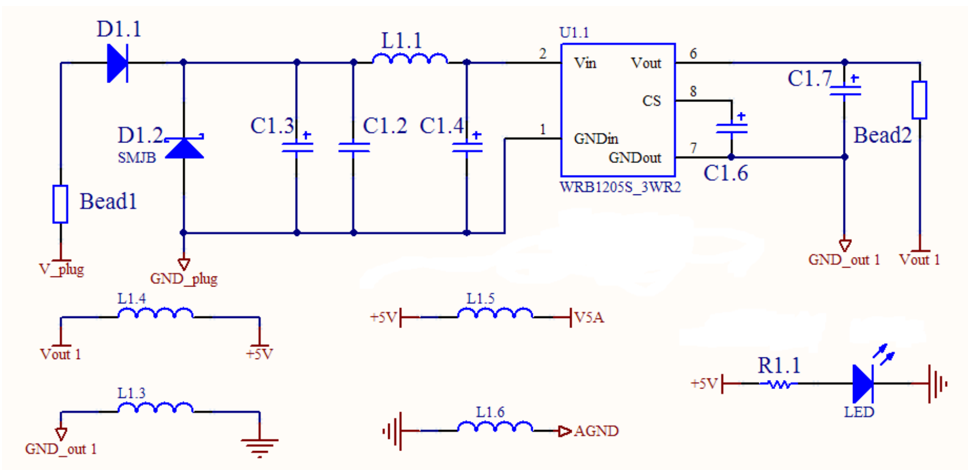

Figure 3. Power circuit.

In Figure 3, Bead1 and Bead2 are the input and output fuses, respectively. Diode D1.1 prevents a reverse current, and D1.2 is a transient voltage suppressor (TVS) with a power of 300~1500 W. C1.3 and C1.7 are input and output filter capacitors, respectively, which remove high-frequency signals.

3.1.3. Supply Rejection Ratio

The actuator mainly includes an air-assisted injector and ignition coil. The ECU determines the current state of the engine according to the sensor signal; analyzes and calculates the optimal injection time, ignition time, injection pulse width, and magnetization pulse width; and drives the injector and ignition coil to achieve accurate control of the engine injection and ignition. The driving circuit designed in this study is shown in Figure 4, and a high-power N-channel MOS tube is used to control the power switching of the electromagnetic coil of the injector.

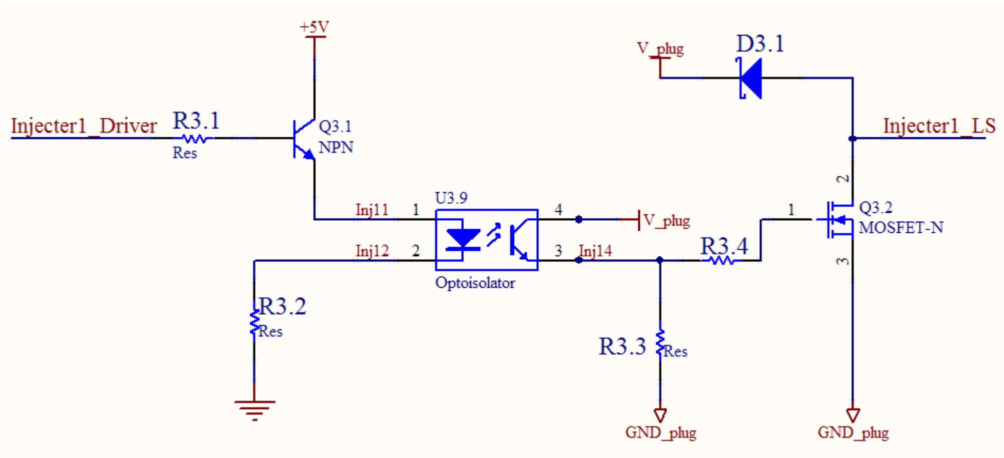

Figure 4. Supply rejection ratio.

3.1.4. Serial Communication Circuit

To monitor the working state of the engine in real time and prepare for the calibration of the engine, the ECU needs to communicate with the monitoring software and calibration software of the host computer. The running state of the engine is transmitted to the host computer software through the serial port. The calibration software transmits the calibration command to the ECU via serial port communication. The serial communication circuit designed in this study is shown in Figure 5.

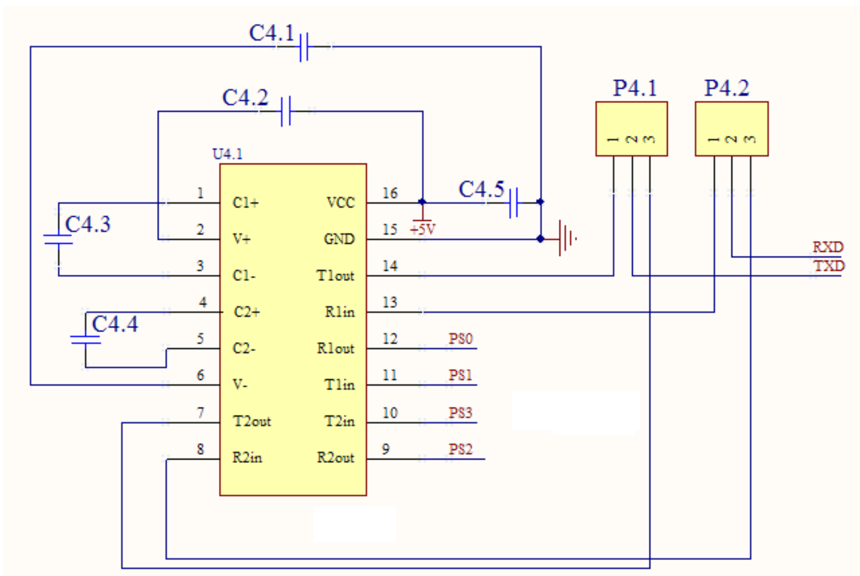

Figure 5. Serial communication circuit.

3.2. Test Machine and Bench

The two-stroke, spark-ignition, kerosene engine is mainly composed of an engine, dynamometer, battery, and fan. Figure 6 shows a structural diagram of the engine test bench. Figure 7 shows the engine bench site. Figure 8 depicts the fuel tank and recorder. Figure 9 shows the oil pipe, oil pump, and oil-pressure-regulating device. Figure 10 shows the cooling device, and Figure 11 depicts the control interface of the whole test bench.

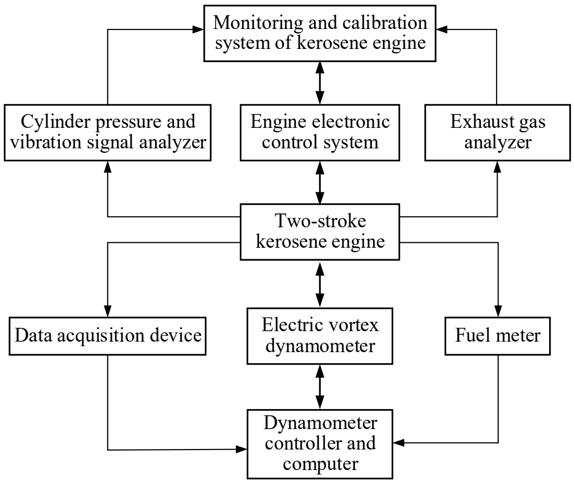

Figure 6. Structure block diagram of the engine test bench.

Figure 7. Engine bench site.

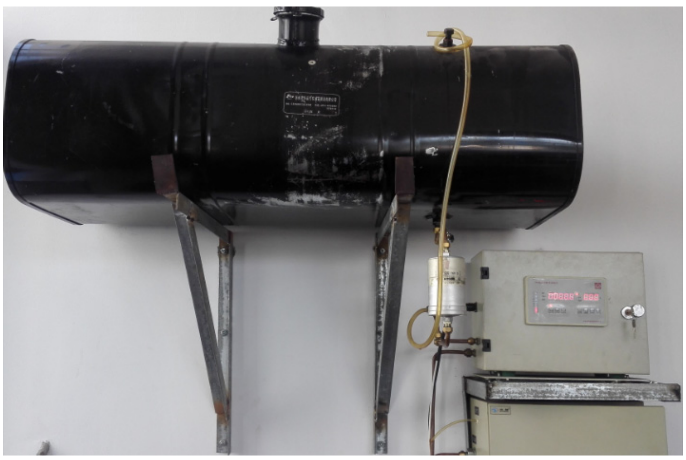

Figure 8. Fuel tank and recorder.

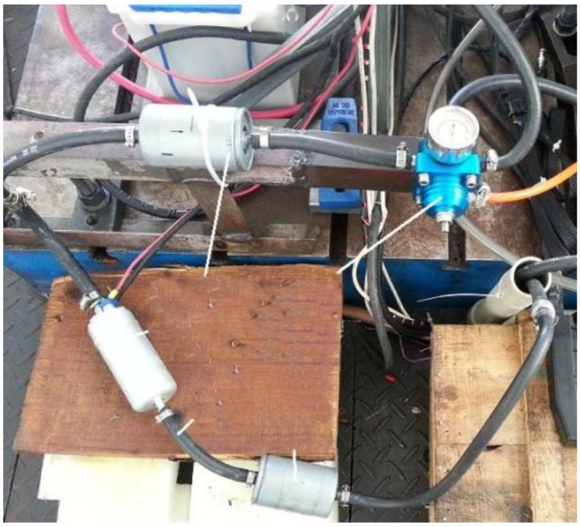

Figure 9. Tubing/oil pump/oil pressure regulation.

Figure 10. Cooling device.

Figure 11. Operational interface.

4. Test Scheme and Analysis of Results

4.1. Analysis of Data Acquired under Cold-Start Conditions

A cold start refers to starting an engine at ambient temperature after the engine has been idle for a certain period of time. In the test, the ambient temperature is set to 13 °C, the battery voltage is 12.4 V, the peak speed of the starting motor is 1200 r/min, and no other auxiliary starting measures are defined during the startup. The startup is divided into four stages, as shown in Figure 12: dragging, starting, stabilizing, and warming up.

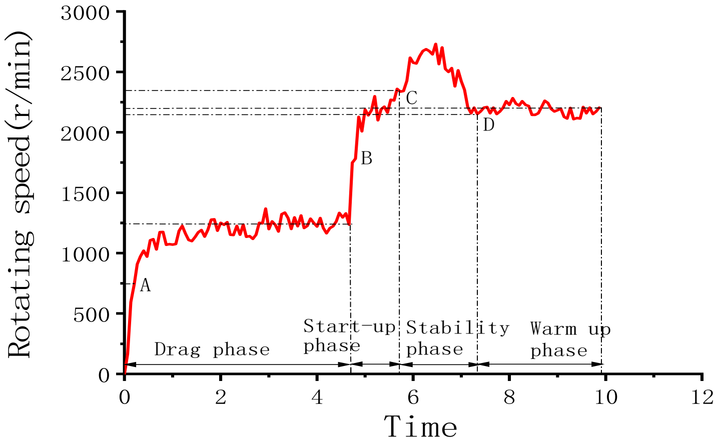

Figure 12. Cold-start phase of the engine.

In this study, the target speed of the cold start is set to 2000 r/min. When the engine speed reaches 2000 r/min, the engine startup stage is considered to be over. The sum of the durations of the engine-drag phase and the start phase is counted as the cold-start time, that is, the time from the start of motor rotation to the first time the engine speed reaches 2000 r/min.

4.1.1. Influence of the Concentration on the Cold-Start Conditions

During a cold start, due to the low temperature in the cylinder, the friction resistance during the engine operation is large, and the combustion conditions are poor. An optimized starting concentration is necessary for a successful start. The concentration coefficient τ_0 is the ratio of the fuel supply in the dragging stage and the starting stage to the fuel supply in the stable stage during a cold start. The formula is as follows:

$$\tau_0 = \frac{V_{drag} + V_{start}}{V_{stable}} \tag{1}$$

V_{drag} is the fuel supply in the dragging phase, V_{start} is the fuel supply in the starting phase, and V_{stable} is the fuel supply in the stable phase.

Keeping the concentration coefficient in the stable stage constant, the concentration coefficients are set to 1, 1.5, 2, 3.5, and 4.5. Figure 13 shows the rotation speed curves for different concentration coefficients during a cold start. Figure 14 shows the engine cold-start time corresponding to different concentration coefficients.

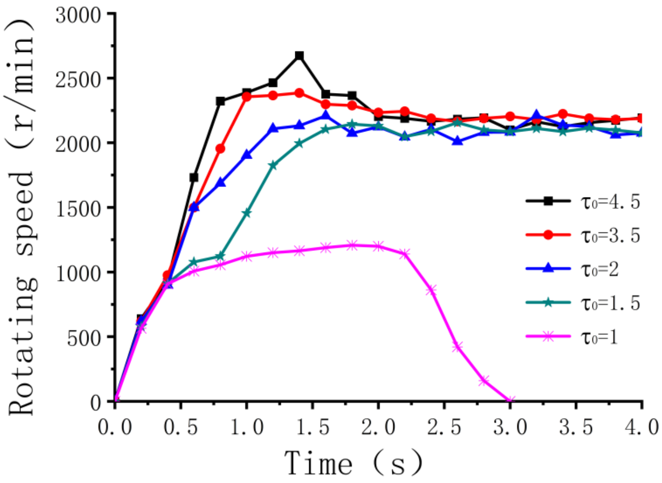

Figure 13. Rotation speed curves for different concentration coefficients during a cold start.

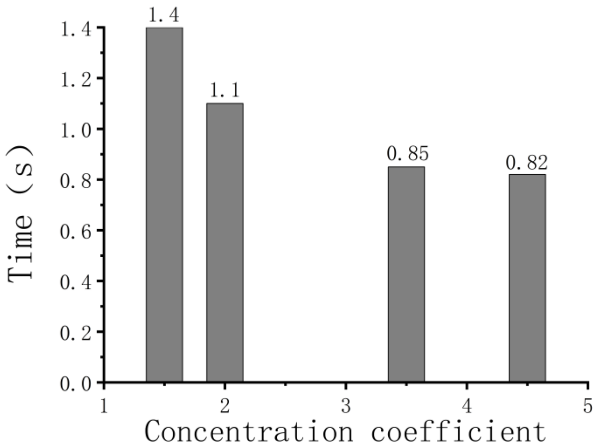

Figure 14. Engine cold-start time under different enrichment coefficients.

Figure 13 shows that when the concentration factor is 1, the flameout is caused by an insufficient oil supply, and the engine can be successfully started when the concentration factor is 1.5 and above. Figure 14 shows that as the concentration coefficient increases, the time needed for the cold start gradually decreases. When the concentration reaches a certain level, the effect on the start time decreases, and the fuel consumption increases. Therefore, the recommended concentration coefficient is set to 3.5.

4.1.2. Influence of the Oil–Air Interval on the Cold-Start Conditions

The oil–gas interval refers to the delay between the opening of the jet valve and the closing of the injector. The oil–air interval is set to 2 ms, 4 ms, 6 ms, 8 ms, and 10 ms. Figure 15 shows the rotation speed for different oil–air intervals during a cold start, and Figure 16 shows the correspondence curves for different oil–air intervals and cold-start times.

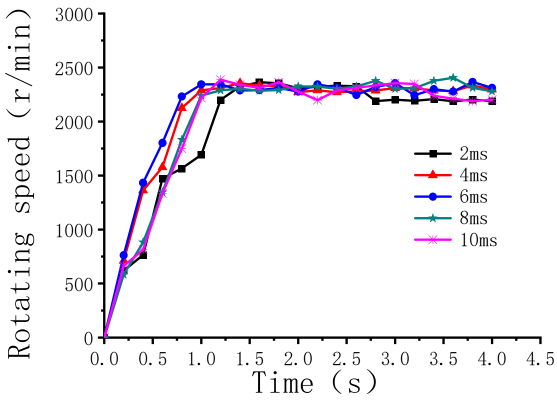

Figure 15. Rotation speeds for different oil–gas intervals during a cold start.

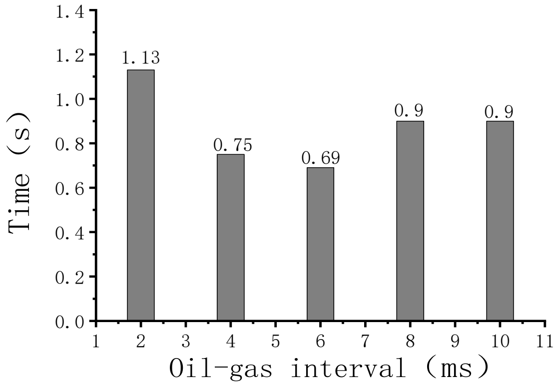

Figure 16. Correspondence curves for different oil–gas intervals and cold-start times.

As seen from Figure 15, the cold-start time is different with different oil–air intervals, while the speed of the warm-up stage tends to be consistent. From Figure 16, it can be seen that the cold-start time is longer when the oil and gas intervals are 2 ms and 10 ms, respectively, and the shortest cold-start time occurs when the interval is 6 ms, which reflects the quality of fuel atomization to a certain extent.

4.1.3. Influence of Ignition Energy on a Cold Start

Increasing ignition energy is an important measure that can be taken to address problems with a cold start. Inductive ignition is adopted, and the magnetization pulse width is set to 1 ms, 2 ms, 3 ms, 4 ms, and 5 ms. Figure 17 shows the rotation speed at different magnetization pulse widths in a cold start, and Figure 18 shows the correspondence curves for different magnetization pulse widths and cold-start times.

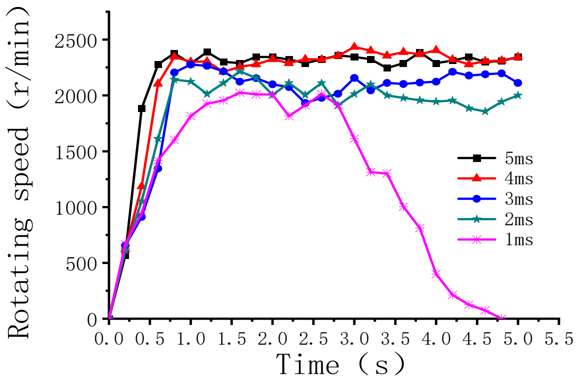

Figure 17. Rotation speed for different magnetization pulse widths during a cold start.

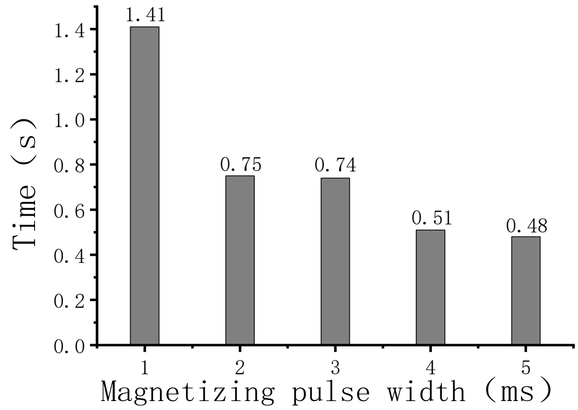

Figure 18. Correspondence curves for different magnetization pulse widths and cold-start times.

Figure 17 shows that in the dragging stage and the starting stage, the slope of the velocity curve increases with increasing magnetization pulse width, indicating that the greater the ignition energy is, the greater the acceleration is. When the magnetization pulse width is 1 ms, the engine speed fluctuates greatly during the starting process, and the ignition is extinguished after starting. Figure 18 shows that increasing the magnetization pulse width of the engine can reduce the cold-start time.

4.2. Influence of the Control Parameters on the Engine Performance at Low Load

4.2.1. Effect of the Ignition Advance Angle and Ignition Energy on the Engine Performance

Under indoor environmental conditions, the relative humidity is 47%, the pressure is 101 kPa, and the cooling water temperature is 85~100 °C. The excess air coefficient α and the fuel injection parameters are adjusted online. The exhaust temperature is the temperature of the sensor at the exhaust pipe, and the specific ignition parameters are shown in Table 6.

Table 6. Ignition parameters at low load.

Parameter	Condition 1	Condition 2
Type of combustion	Kerosene	Kerosene
Rotation speed (r/min)	3000	3000
Throttle opening angle	14%	16%
Advance angle of ignition (°BTDC)	15~35	15~35
Magnetization time (ms)	2~6	2~6
Injection end angle (°BTDC)	50	70
Injection quantity (mg)	8.4	8.4
Excess air coefficient	0.9–1.1	0.9–1.1

The engine power, fuel consumption rate, exhaust temperature, and HC, CO, and CO_2 emission curves obtained from the test under Condition 1 are shown in Figures 19–24.

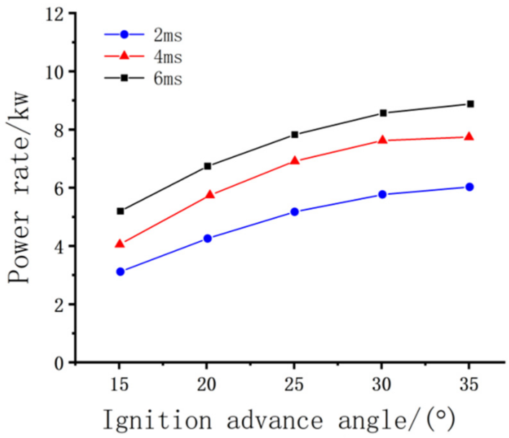

Figure 19. Influence of the ignition parameters on engine power.

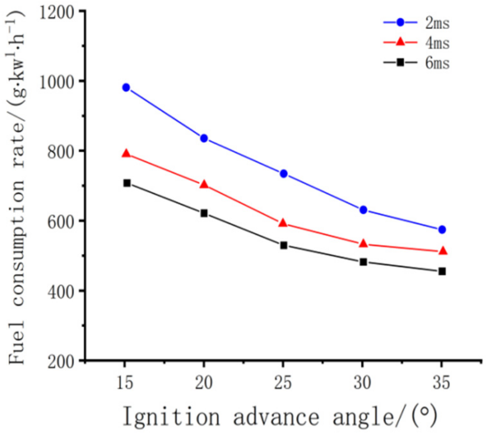

Figure 20. Effect of the ignition parameters on fuel consumption.

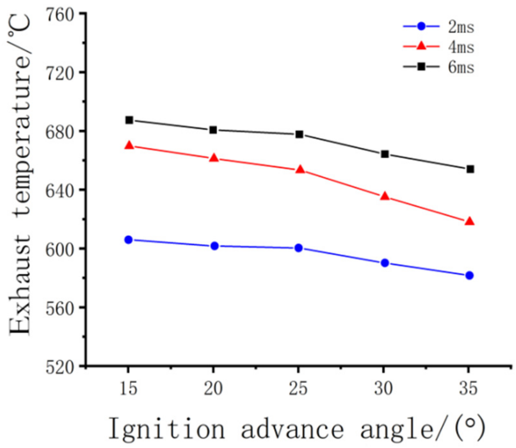

Figure 21. Influence of the ignition parameters on exhaust temperature.

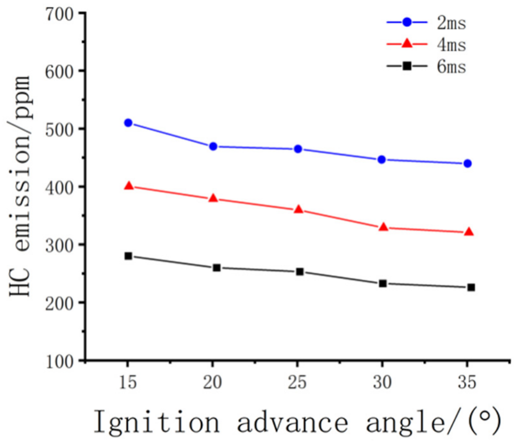

Figure 22. Effect of the ignition parameters on HC emissions.

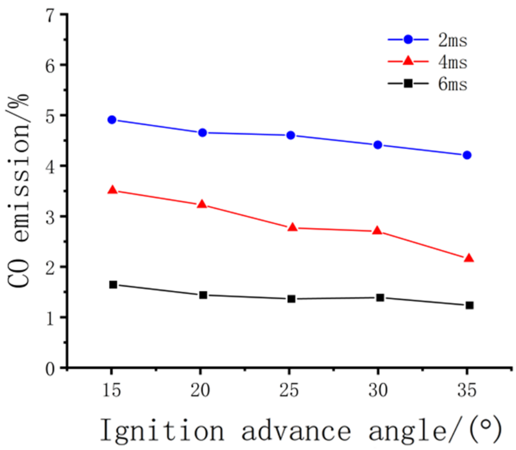

Figure 23. Effect of the ignition parameters on CO emissions.

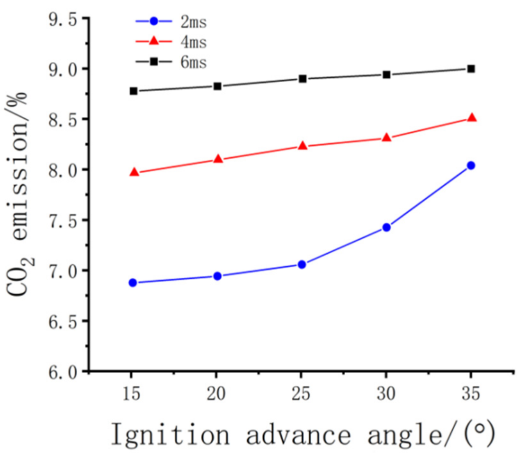

Figure 24. Effect of the ignition parameters on CO_2 emissions.

Figures 19–21 show that at the same magnetization pulse width, as the ignition advance angle gradually increases, the engine power gradually increases, while the fuel consumption and exhaust temperature gradually decrease. The reason is that if the ignition duration is short, and ignition occurs relatively late, the piston moves down when the mixture starts to burn, increasing the cylinder volume and reducing the combustion pressure. Figures 22–24 show that when the injection pulse width increases from 2 ms to 6 ms, the HC and CO emissions decrease, while the CO_2 emissions gradually increase. These changes are mainly due to the low ignition energy produced by the small magnetization pulse width, the difficulty in igniting kerosene fuel, and the insufficient combustion of the in-cylinder mixture, resulting in an unanticipated increase in HC and CO but a decrease in CO_2.

The engine power, fuel consumption rate, exhaust temperature, and HC, CO, and CO2 emission curves obtained from the test under Condition 2 are shown in Figures 25–30.

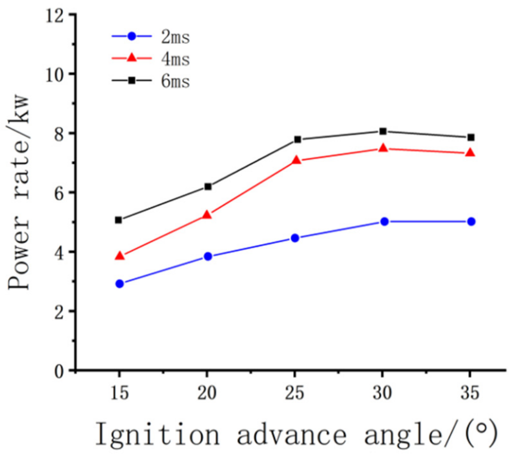

Figure 25. Influence of the ignition parameters on engine power.

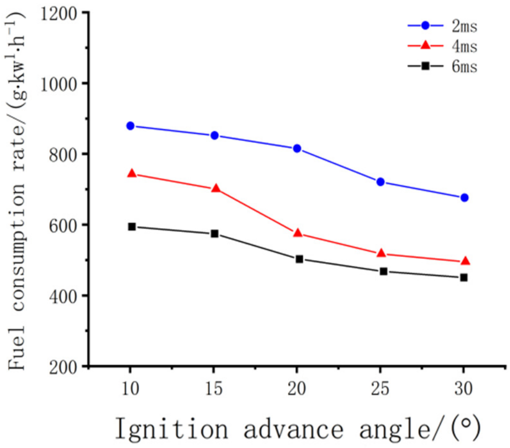

Figure 26. Effect of the ignition parameters on fuel consumption.

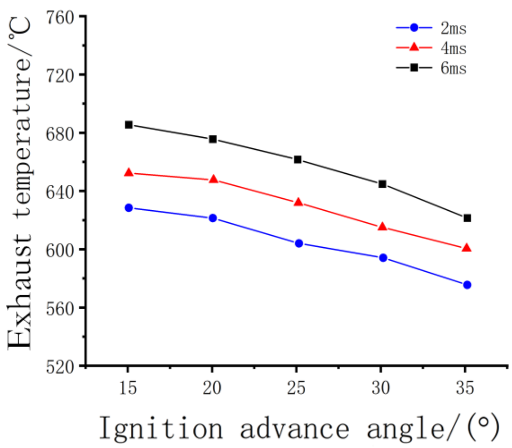

Figure 27. Influence of the ignition parameters on exhaust temperature.

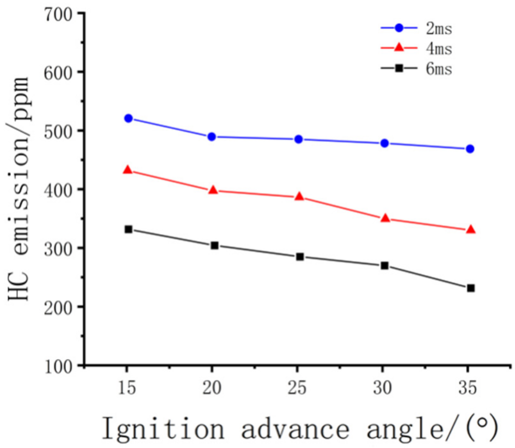

Figure 28. Effect of the ignition parameters on HC emissions.

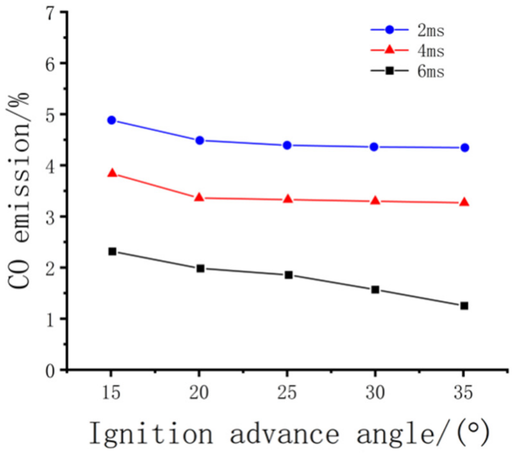

Figure 29. Effect of the ignition parameters on CO emissions.

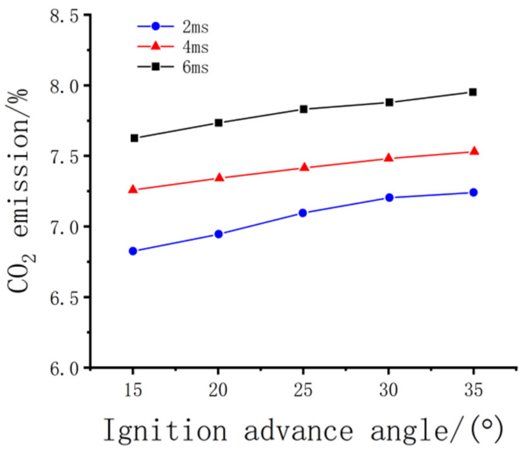

Figure 30. Effect of the ignition parameters on CO_2 emissions.

Figures 25–30 show that at the same magnetization pulse width, as the ignition advance angle gradually increases, the engine power and CO_2 emissions gradually increase, while the fuel consumption rate, exhaust temperature, and HC and CO emissions gradually decrease. Appropriately increasing the ignition advance angle within a certain range will have an improvement effect, fully burning in the cylinder, and HC and CO will be appropriately reduced [18,19]. Combined with the test results under Condition 1, these results show that the appropriate ignition time can improve the combustion in the cylinder of the engine.

4.2.2. Effects of the Injection End Angle and Injected Fuel Quantity on Engine Performance

The ambient settings are the same as those described in Section 4.2.1. The ignition parameters of the engine are shown in Table 7.

Table 7. Ignition parameters under low-load conditions.

Parameter	Condition 3	Condition 4
Type of combustion	Kerosene	Kerosene
Rotation speed (r/min)	3000	3000
Throttle opening angle	14%	16%
Advance angle of ignition (°BTDC)	25	30
Magnetization time (ms)	5	5
Injection end angle (°BTDC)	40~70	40~70
Injection quantity (mg)	7.5~8.5	7.5~8.5
Excess air coefficient	0.9–1.1	0.9–1.1

The engine power, fuel consumption rate, exhaust temperature, and HC, CO, and CO_2 emission curves obtained from the test under Condition 3 are shown in Figures 31–36.

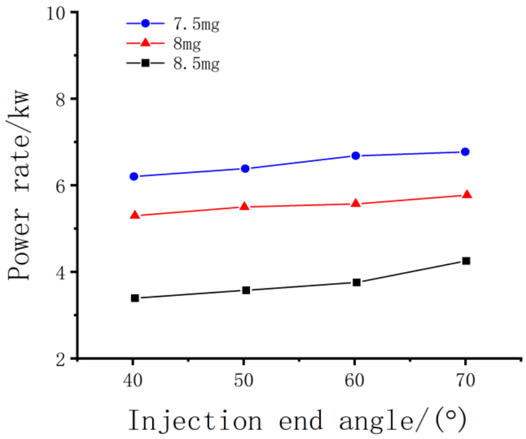

Figure 31. Effect of the injection parameters on engine power.

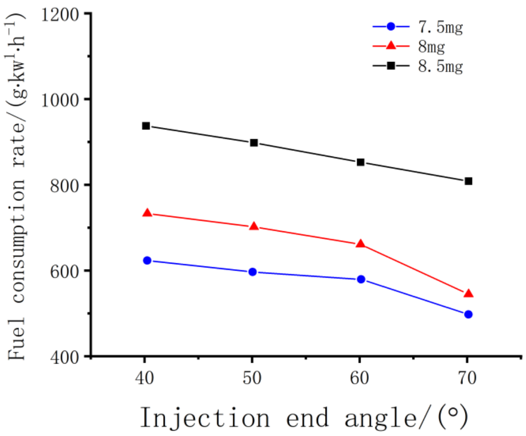

Figure 32. Effect of the injection parameters on fuel consumption.

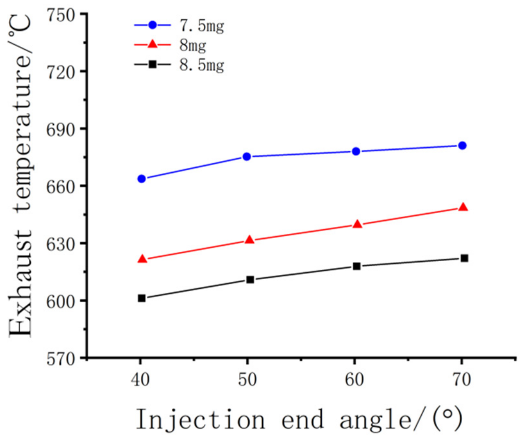

Figure 33. Effect of the injection parameters on exhaust temperature.

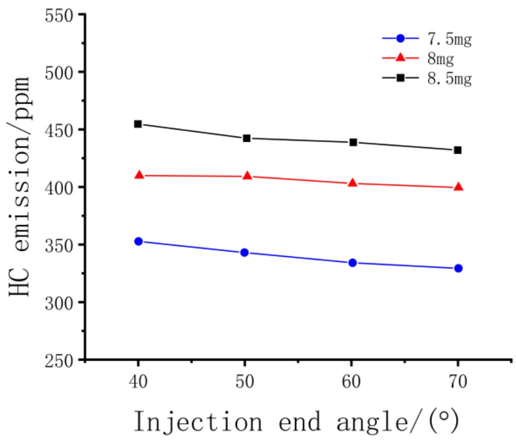

Figure 34. Effect of the injection parameters on HC emissions.

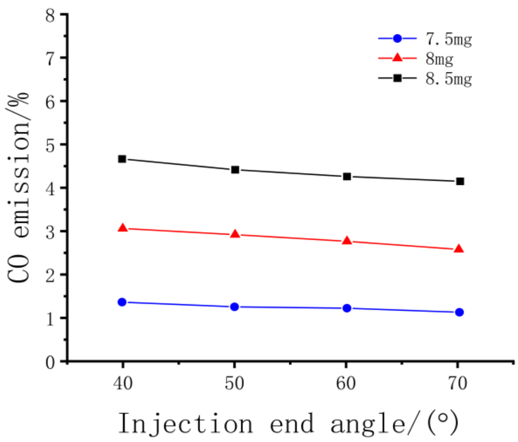

Figure 35. Effect of the injection parameters on CO emissions.

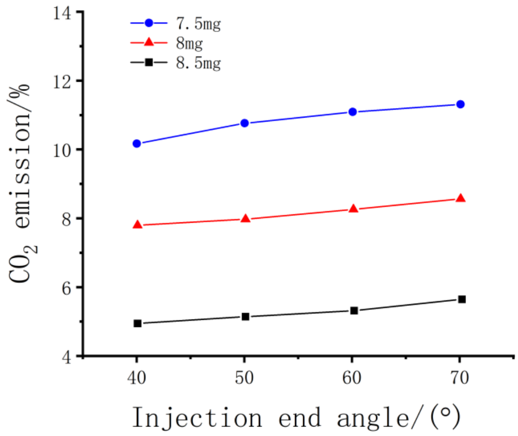

Figure 36. Effect of the injection parameters on CO_2 emissions.

Figures 31–36 show that with increasing injected fuel, the engine power, exhaust temperature, and CO_2 emissions increase, while the fuel consumption and HC and CO emissions decrease. The main reason is that a proper ignition advance angle can completely mix the oil and gas to ensure complete combustion, and a proper delay of the injection end angle can increase HC and CO emissions.

The power, fuel consumption, exhaust temperature, and pollutant emission curves of the engine are obtained under operating condition 4, as shown in Figures 37–42, respectively.

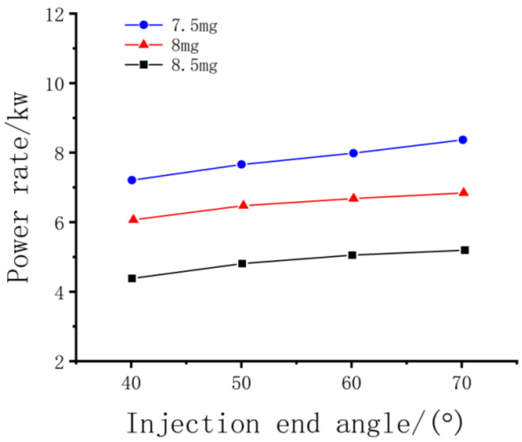

Figure 37. Effect of the injection parameters on engine power.

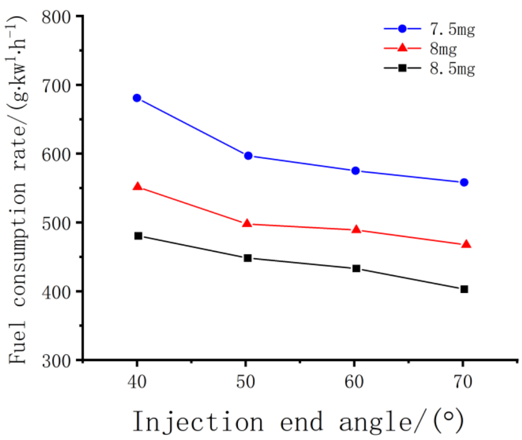

Figure 38. Effect of the injection parameters on fuel consumption.

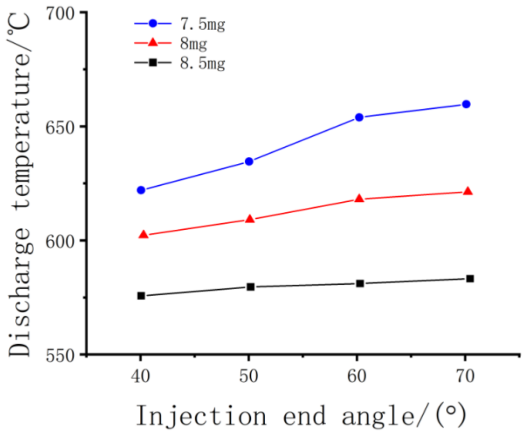

Figure 39. Effect of the injection parameters on exhaust temperature.

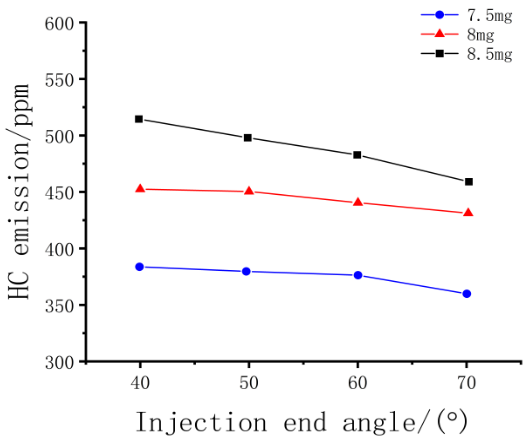

Figure 40. Effect of the injection parameters on HC emissions.

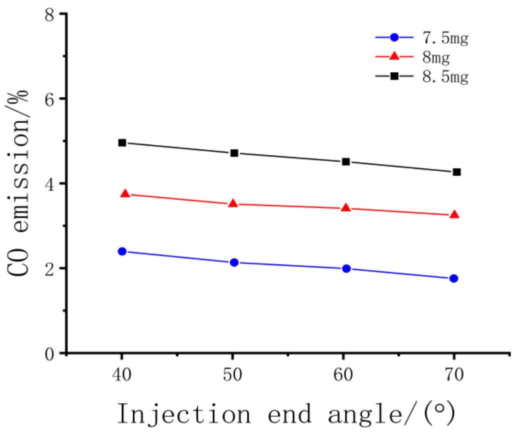

Figure 41. Effect of the injection parameters on CO emissions.

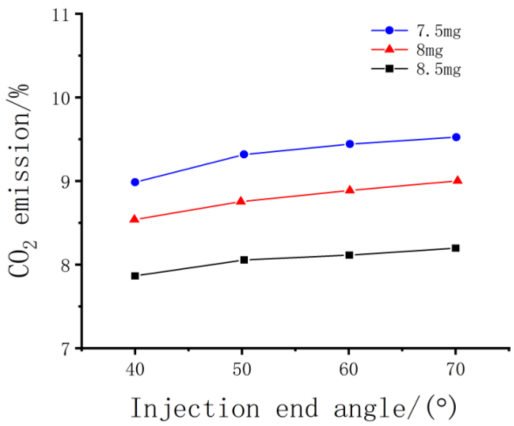

Figure 42. Effect of the injection parameters on CO_2 emissions.

Figures 37–42 show that with the increase in the injection end angle, the power, exhaust temperature, and CO_2 emissions of the engine increase, while the fuel consumption and HC and CO emissions decrease. The pollutant emissions are lowest when the injection volume is 7.5 mg and the excess air coefficient is approximately 1.1.

5. Conclusions

In this study, experimental research is carried out under cold-start conditions and small-load conditions, and the conclusions are as follows:

(1) The ambient temperature is set to 13 °C, the battery voltage is set to 12.4 V, and the peak speed of the starting motor is set to 1200 r/min.

① The enrichment coefficients are sequentially set to 1, 1.5, 2, 3.5, and 4.5. As the enrichment coefficient increases, the cold-start time decreases. After reaching a certain concentration, the amplitude decreases, while the fuel consumption increases.

② The oil–gas interval is sequentially set to 2 ms, 4 ms, 6 ms, 8 ms, and 10 ms, and there is a quadratic relationship between the oil–gas interval and the cold-start time. The required cold-start time is the smallest when the oil–gas interval is 6 ms.

③ The magnetization pulse width is sequentially set to 1 ms, 3 ms, 4 ms, and 5 ms, and, as the magnetization pulse width increases, the cold-start time decreases.

(2) The ambient temperature is set at 25 °C, the relative humidity at 47%, the pressure at 101 kPa, the cooling water temperature at 85~1~100 °C, the rotation speed at 3000 r/min, and the throttle opening at 14% to 16%.

① The injection end angles are set to 50° and 70° BTDC. As the ignition advance angle increases, the power and CO_2 emissions also increase, while the fuel consumption, exhaust temperature, and HC and CO emissions gradually decrease. The ignition energy exerts a great influence on the performance of the engine. A larger ignition energy can improve the combustion in the engine cylinder and increase the output power.

② The ignition advance angle is set to 25° and 30° BTDC. Moderately increasing the injection end angle can improve the engine's power, fuel consumption, and HC and CO emissions. A lean mixture makes the combustion more efficient and decreases the emission of pollutants.

Author Contributions: Conceptualization, B.L., T.B., and R.L.; software, N.L. and Y.L. (Ying Luo); formal analysis, B.L. and T.B.; investigation, B.L., R.L., and N.L.; resources, T.B. and R.L.; writing—original draft preparation, B.L. and T.B.; writing—review and editing, T.B., B.L., R.L., and Y.L. (Yuchen Liu); supervision, T.B. and B.L.; funding acquisition, T.B. All authors have read and agreed to the published version of the manuscript.

Funding: This research is supported by the National Scholarship Fund (202008370131), Key R&D Projects in Shandong Province (2019GGX104056), and the Doctoral Research Fund of Shandong Jianzhu University (X18067Z).

Institutional Review Board Statement: Not applicable.

Informed Consent Statement: Not applicable.

Data Availability Statement: All data used to support the findings of this study are included within the article.

Conflicts of Interest: The authors declare that they have no known competing financial interests or personal relationships that could have appeared to influence the work reported in this paper.

References

1. Crosbie, S.C.; Polanka, M.D.; Litke, P.; Hoke, J.L. Increasing Reliability of a Two-Stroke internal combustion engine for dynamically changing altitudes. *J. J. Propuls. Power* **2015**, *30*, 87–95. [CrossRef]
2. Feng, Y.; Wang, H.; Gao, R. A zero-dimensional mixing controlled combustion model for real time performance simulation of marine two-stroke diesel engines. *Energies* **2019**, *12*, 2000. [CrossRef]
3. Brusiani, F.; Falfari, S.; Forte, C.; Cazzoli, G.; Verziagi, P.; Ferrari, M.; Catanese, D. Definition of a CFD Methodology to evaluate the cylinder temperature distribution in two-stroke air cooled engines. *J. Energy Procedia* **2015**, *81*, 765–774. [CrossRef]
4. Uyumaz, A.; Solmaz, H.; Yılmaz, E.; Yamik, H.; Polat, S. Experimental examination of the effects of military aviation fuel JP-8 and biodiesel fuel blends on the engine performance, exhaust emissions and combustion in a direct injection engine. *J. Fuel Process. Technol.* **2014**, *128*, 158–165. [CrossRef]
5. Lu, Y.; Pan, J.; Fan, B.; Otchere, P.; Chen, W.; Cheng, B. Research on the application of aviation kerosene in a direct injection rotary engine–Part 2: Spray combustion characteristics and combustion process under optimized injection strategies. *J. Energy Convers. Manag.* **2020**, *203*, 112217. [CrossRef]
6. Schihl, P.; Hoogterp-Decker, L. On the ignition behavior of JP-8 in military relevant diesel engines. *J. SAE Int. J. Engines* **2011**, *4*, 1–13. [CrossRef]
7. Szymkowicz, P.G.; Benajes, J. Development of a diesel surrogate fuel library. *Fuel* **2018**, *222*, 21–34. [CrossRef]
8. Ma, H.; Xie, M.; Zeng, W.; Chen, B. Experimental study on combustion characteristics of chinese RP-3 kerosene. *Chin. J. Aeronaut.* **2016**, *29*, 375–385. [CrossRef]
9. Hu, J.; Liu, B.; Zhang, C.; Gao, H.; Zhao, Z.; Zhang, F.; Wang, Y. Experimental study on the spray characteristics of an air-assisted fuel injection system using kerosene and gasoline. *Fuel* **2019**, *235*, 782–794. [CrossRef]
10. Damanik, N.; Ong, H.C.; Chong, W.; Mahlia, T.M.; Silitonga, A.S. A review on the engine performance and exhaust emission characteristics of diesel engines fueled with biodiesel blends. *Environ. Sci. Pollut. Res.* **2018**, *25*, 15307–15325. [CrossRef] [PubMed]
11. Qiu, J.; Pan, C.; Zhou, M. Simulation of fuel spray and combustion of compression ignition heavy-oil engine. In Proceedings of the 2016-AIAA Modeling and Simulation Technologies Conference, Washington, DC, USA, 13–17 June 2016. [CrossRef]
12. He, Y.; Hu, C.; Liu, N.; Zhang, Z.; Su, S. Experiment on cold start performance of a spark-ignition aviation kerosene direct injection engine. *J. Trans. CSICE* **2022**, *40*, 54–61. [CrossRef]
13. Wang, H.; Yang, Y.; Zhang, L.; Chen, Y.; Zhou, Y.; Zheng, Z.; Yao, M. Numerical investigation on combustion system optimization for direct injection of aviation kerosene in a two-stroke SI engine for unmanned aerial vehicle. *Fuel* **2022**, *329*, 125452. [CrossRef]
14. Liu, R.; Huang, K.; Qiao, Y.; Wang, Z.; Ji, H. Combustion Performance Investigation of Aviation Kerosene (RP-3) on a Compression Ignition Diesel Engine Under Various Loads. *J. Energy Resour. Technol.* **2022**, *144*, 032308. [CrossRef]
15. Liu, R.; Wei, M.; Yang, H.; Wang, Y.; Bei, T. Cold start control strategy of a two-stroke direct injection spark-ignited kerosene engine. *J Aerosp. Power.* **2017**, *32*, 213–220. [CrossRef]
16. Hamza, N.H.; Ekaab, N.S.; Chaichan, M.T. Impact of using Iraqi biofuel–kerosene blends on coarse and fine particulate matter emitted from compressionignition engines. *J. Alex Eng. J.* **2020**, *59*, 166–174. [CrossRef]
17. Ashour, M.K.; Elwardany, A. Addition of two kerosene-based fuels to diesel-biodiesel fuel: Effect on combustion, performance and emissions characteristics of CI engine. *Fuel* **2020**, *269*, 117473. [CrossRef]
18. Huang, H.; Li, Z.; Teng, W.; Zhou, C.; Huang, R.; Liu, H.; Pan, M. Influence of n-butanol-diesel-$PODE_{3\text{-}4}$ fuels coupled pilot injection strategy on combustion and emission characteristics of diesel engine. *Fuel* **2019**, *236*, 313–324. [CrossRef]
19. Chen, Y.; Zhu, Z.; Chen, Y.; Huang, H.; Zhu, Z.; Lv, D.; Pan, M.; Guo, X. Study of injection pressure couple with EGR on combustion performance and emissions of natural gas-diesel dual-fuel engine. *Fuel* **2020**, *261*, 116409. [CrossRef]